

# MESTI-MEGANet: Micro-expression Spatio-Temporal Image and Micro-expression Gradient Attention Networks for Micro-expression Recognition

Luu Tu Nguyen\*, Vu Tram Anh Khuong\*, Thanh Ha Le\*, Thi Duyen Ngo\*

\*Faculty of Information Technology, VNU University of Engineering and Technology, Ha Noi, Viet Nam

**Abstract**—Micro-expression recognition (MER) is a challenging task due to the subtle and fleeting nature of micro-expressions. Traditional input modalities, such as Apex Frame, Optical Flow, and Dynamic Image, often fail to adequately capture these brief facial movements, resulting in suboptimal performance. In this study, we introduce the Micro-expression Spatio-Temporal Image (MESTI), a novel dynamic input modality that transforms a video sequence into a single image while preserving the essential characteristics of micro-movements. Additionally, we present the Micro-expression Gradient Attention Network (MEGANet), which incorporates a novel Gradient Attention block to enhance the extraction of fine-grained motion features from micro-expressions. By combining MESTI and MEGANet, we aim to establish a more effective approach to MER. Extensive experiments were conducted to evaluate the effectiveness of MESTI, comparing it with existing input modalities across three CNN architectures (VGG19, ResNet50, and EfficientNetB0). Moreover, we demonstrate that replacing the input of previously published MER networks with MESTI leads to consistent performance improvements. The performance of MEGANet, both with MESTI and Dynamic Image, is also evaluated, showing that our proposed network achieves state-of-the-art results on the CASMEII and SAMM datasets. The combination of MEGANet and MESTI achieves the highest accuracy reported to date, setting a new benchmark for micro-expression recognition. These findings underscore the potential of MESTI as a superior input modality and MEGANet as an advanced recognition network, paving the way for more effective MER systems in a variety of applications.

**Index Terms**—Micro-expression Spatio-Temporal Image, gradient attention, micro-expression, micro-expression recognition, micro-expression input modality, micro-expression recognition network.

## I. INTRODUCTION

Facial expression, a vital channel of non-verbal communication, encompasses two primary types: macro expressions and micro expressions. Macro expressions are typically deliberate, easily observable, and last for an extended period, conveying a person's emotions openly [1]. In contrast, micro expressions (ME) are brief, involuntary facial movements that last less than 0.5 seconds [2], [3], making them significantly challenging to control or fabricate. Unlike macro expressions, micro expressions reveal a person's genuine emotions, often surfacing when one attempts to conceal their true feelings

[4]. These fleeting expressions are especially revealing in high-risk situations [5], [6], where concealing emotions is common. Since these unique characteristics of micro expressions, they have garnered significant attention as a channel for uncovering individuals' genuine thoughts and emotions. Their involuntary nature provides valuable insights, making them highly applicable in a range of critical fields. For instance, micro-expressions play a crucial role in enhancing the accuracy of deception detection systems, providing valuable insights that more prolonged expressions may not capture [7]. In criminal investigations, law enforcement officers can assess a suspect's truthfulness by analyzing micro-expressions that may contradict verbal statements [8]. Beyond security applications, micro-expressions are increasingly relevant in healthcare, particularly in clinical settings, where they can provide essential clues about a patient's emotional state and aid medical professionals in assessing recovery progress [9].

Despite its potential, micro-expression recognition (MER) presents significant challenges due to the brevity and subtle intensity of micro-expressions. Studies have shown that even experts achieve only 47% accuracy in recognizing micro-expressions, highlighting the inherent complexity of this task [10]. However, leveraging advancements in computational capabilities, as well as modern machine learning and deep learning algorithms, computer-based systems for micro-expression analysis have demonstrated significant superiority over human performance, with accuracy rates often exceeding 50%. These advancements offer a promising pathway for achieving more accurate and reliable recognition of micro-expressions across a wide range of applications [11].

Early MER approaches primarily relied on handcrafted features and machine learning techniques. These handcrafted features can generally be classified into two main categories: those that capture variations in facial texture and those that focus on variations in facial illumination. A foundational texture-based approach utilized Local Binary Patterns on Three Orthogonal Planes (LBP-TOP) [33], extending the LBP operator [18] to capture spatiotemporal features from facial videos. Building upon LBP-TOP, various enhancements were introduced to better capture subtle dynamic texture changes, including the use of second-order Gaussian jets [19], LBP Six Intersection Points (LBP-SIP) [20], Space-Time LBP (STLBP) [21], and Space-Time Completed Local Quantized

Patterns (STCLQP) [22]. These advancements aimed to refine the representation of facial texture variations over time. In contrast, for illumination-based analysis, optical flow [24] derived methods have been extensively studied. Directional Mean Optical Flow (MDMO) [25], Bi-weighted Oriented Optical Flow (Bi-WOOF) [26], and Fuzzy Optical Flow Directional Histograms (FHOFO) [27] have been proposed to capture subtle changes in facial illumination and motion.

While these handcrafted approaches (both texture and illumination-based) provided a crucial baseline, they remained limited due to their restricted accuracy and the complex feature extraction process required. Previous surveys [11], [23] have shown that the accuracy of handcrafted features combined with machine learning ranges from approximately 40-60%, depending on the dataset and evaluation protocol used. In contrast, deep learning-based methods have demonstrated superior performance in MER. Currently, deep learning-based MER methods are considered state-of-the-art [11], therefore, this study focuses on leveraging deep learning approaches.

Within the context of deep learning for MER, two key factors play a pivotal role in determining system performance: input modalities and network architecture [11]. Input modalities for MER can be broadly classified into three categories: (1) Static Images, (2) Optical Flow, and (3) Dynamic Imaging Techniques. Each modality presents distinct advantages and challenges, and their selection significantly impacts the overall effectiveness of MER systems.

**Static Images:** Static image-based approaches often utilize the apex frame, which represents the peak intensity of a micro-expression. This method reduces the complexity of video data by condensing an entire sequence into a single frame, thereby decreasing computational overhead. However, static images lack temporal information, which is crucial for identifying micro-expressions characterized by their rapid onset and offset. The absence of these temporal cues may lead to misclassification, as the system cannot discern the subtle temporal changes critical for distinguishing micro-expressions. Consequently, static image-based MER systems often exhibit suboptimal accuracy [12], [13].

**Optical Flow:** Optical flow, a widely used technique for motion representation, provides both the magnitude and direction of pixel movement through a two-dimensional vector field comprising horizontal and vertical flows. This method introduces temporal information into the analysis, enhancing the system's ability to capture micro-expression dynamics. However, the effective integration of optical flow in MER systems often requires the design of multi-stream network architectures to process both horizontal and vertical flow components. Additionally, optical flow techniques are susceptible to noise caused by lighting variations, head movements, and other extraneous factors, potentially impairing recognition accuracy. [17], [27]

**Dynamic Imaging Methods:** Dynamic imaging methods summarize a video sequence into a single image that encodes temporal information. A notable example of this technique is the Dynamic Image [28], which represents a video as a single image capturing the overall temporal essence of the sequence. This method has been shown to be effective in action

recognition tasks, as demonstrated by the original authors. Subsequently, it has been adapted for micro-expression recognition (MER) in several studies [15], [56]. However, the direct inheritance of this technique from action recognition tasks has limited its effectiveness in MER, as it struggles to accurately capture the subtle and minute facial movements characteristic of micro-expressions. Recognizing the inadequacy of existing input representations for MER, some researchers have attempted to refine dynamic imaging techniques specifically for this domain. For instance, Affective Image [32] and Active Image [16] are examples of efforts to tailor dynamic imaging approaches to better suit MER tasks. While these studies made progress in adapting the dynamic image concept, their input representations remain limited in comprehensiveness. Both approaches designed specialized networks for their respective inputs, yet the recognition accuracy of these networks has remained constrained, achieving only 50–60% on four-class classification tasks, rather than the five-class standard used in earlier research.

In summary, existing input modalities fail to comprehensively address the challenges of micro-expression recognition. Static images, while computationally efficient, lack temporal information critical for capturing transient micro-movements. Optical flow, though effective in encoding motion, struggles to represent the subtle intensity and brevity of micro-expressions, often resulting in noisy estimations due to their low-amplitude characteristics. These limitations underscore the pressing need for a modality that seamlessly integrates nuanced spatio-temporal motion cues into a compact and discriminative representation, tailored specifically for micro-expression dynamics.

On the other hand, although Convolutional Neural Networks (CNN) have demonstrated effectiveness in extracting spatial features from facial expressions, they face notable limitations when applied to MER. Traditional CNN architectures tend to focus on features with prominent magnitudes, often overlooking the extremely subtle and transient motion signals inherent in micro-expressions. This underrepresentation of fine-grained motion details reduces the model's ability to distinguish between different micro-expressions, particularly when the movements are brief and of low intensity. These challenges highlight the need for more specialized architectures and input representations that can effectively capture and amplify subtle motion cues.

Previous studies have proposed various network architectures to address these limitations, yet significant gaps remain. For instance, MER-GCN [53] employs Graph Convolutional Networks (GCNs) to model the spatio-temporal relationships between Action Units (AUs). While this approach shows promise, it suffers from high computational complexity and limited generalization across diverse datasets such as SAMM. Additionally, the use of AUs as input modality is suboptimal, as accurately identifying AUs in real-world conditions is still highly challenging. LEARNet [51] utilizes Dynamic Image as input with a standard CNN architecture but lacks a dedicated attention mechanism tailored for micro-movements, leading to the omission of critical features. GEME [56] introduces a multi-task framework that incorporates gender information, but its feature extraction process still fails to fully leverage

subtle gradient variations. AMAN [52] integrates an attention mechanism into CNNs to focus on facial regions; however, this mechanism primarily relies on raw pixel intensity rather than gradient-based motion, making it less effective in detecting low-intensity changes. Similarly, CapsNet [50] and optical flow-based methods using OFF-ApexNet [46] have shown improved accuracy but remain susceptible to noise caused by lighting variations and head movements, particularly for micro-expressions with low amplitude.

These limitations underscore the need for a more robust and efficient approach that can amplify subtle motion informations and direct attention to regions exhibiting significant gradient changes. To address these challenges, in this paper, a novel MER method is proposed that introduces a dynamic input modality called the Micro-expression Spatio-Temporal Image (MESTI). This modality represents a video sequence as a single image by capturing the motion features of micro-expressions. Furthermore, this paper introduces Micro-expression Gradient Attention Networks (MEGANet), a novel network architecture that incorporates a Gradient Attention mechanism. This mechanism leverages gradient information from intermediate layers to highlight regions with subtle motion, thereby enhancing the extraction of fine-grained features that are critical for accurate micro-expression recognition. The contributions of the paper are as follows:

- A novel input modality, MESTI, which represents video sequences as single images that specifically synthesize and highlight micro-movements within micro-expression videos.
- MEGANet: By integrating a novel Gradient Attention Block, we develop a micro-expression network capable of focusing on motion regions, thereby improving the performance of micro-expression recognition.

Through extensive experiments, the effectiveness of each proposed component (MESTI, MEGANet) is demonstrated by evaluating their individual contributions and their combination with previously published methods. The results show that each component of our proposed method enhances the performance of the micro-expression recognition (MER) process, and when combined, MESTI and MEGANet yield a effective overall MER approach.

## II. PROPOSED METHOD

### A. Micro-expression Spatio-Temporal Image

The initial idea for creating an effective input representation for ME stemmed from observing and studying the motion characteristics of micro-expressions. The intensity of motion gradually increases from the onset frame (the starting frame) to the apex (the frame with the highest ME intensity), then decreases towards the offset frame (the final frame representing the ME). Based on this characteristic, the proposed method simulates this motion in the process of constructing a distinctive representation for micro-expressions, namely MESTI. Our objective is to create a spatio-temporal image that effectively represents a micro-expression video. To achieve this, a temporal encoding approach introduced that transforms the entire video sequence into a single representative image.

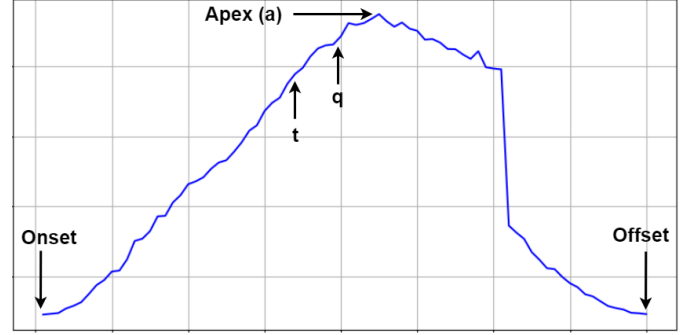


Fig. 1: Motion intensity in ME.

Additionally, our method incorporates the process of aggregating spatial information from the video into a compact static representation.

Inspired by the approximate rank pooling method, which has been used in modeling video evolution [29], a similar strategy is proposed to encode the temporal evolution of micro-expressions into a single image. This approach captures the dynamic variations in facial expressions over time while preserving the spatial structure necessary for effective micro-expression recognition.

1) **Spatial Encoding:** A video is represented as a sequence of consecutive frames, denoted as  $I_1, \dots, I_t, \dots, I_T$ , where  $T$  is the total number of frames, and  $I_t$  represents the frame at time step  $t$ . Let  $\psi(I_t) \in \mathbb{R}^d$  denote the feature vector extracted from each individual frame  $I_t$ . In this study,  $\psi(I_t)$  is a vector that directly encodes the RGB components of each pixel in the frame  $I_t$ .

Let  $d \in \mathbb{R}^d$  be defined as a parameter vector responsible for assigning a score to each frame ( $S(t|d)$ ) at time  $t$  using a ranking function in Equation 1.

$$S(t|d) = \langle d, \psi(I_t) \rangle \quad (1)$$

The parameter  $d$  is learned based on the entire frame sequence, ensuring that the scores assigned to each frame reflect their relative ranking. The learning process of  $d$  is formulated as a convex optimization problem using RankSVM [49],  $d^*$  refers to the optimal parameter vector  $d$  that is learned based on the entire frame sequence, as described in Equation 2.

$$d^* = \rho(I_1, \dots, I_T; \psi) = \arg \min_d E(d) \quad (2)$$

This process integrates spatial information from individual frames into a micro-expression image that preserves structural and appearance details. By leveraging the extracted RGB feature vectors, the method ensures that spatial characteristics of each frame are considered in the ranking process, allowing the network to learn an optimal frame-ordering that reflects their relative importance in the sequence.

2) **Temporal Encoding:** Temporal encoding is performed based on the characteristic motion patterns of micro-expressions, which serve as a basis for assigning scores to each frame during the rank pooling process of spatial encoding. Figure 1 illustrates the intensity of motion in ME. The motion characteristics of micro-expressions can be easily observed:

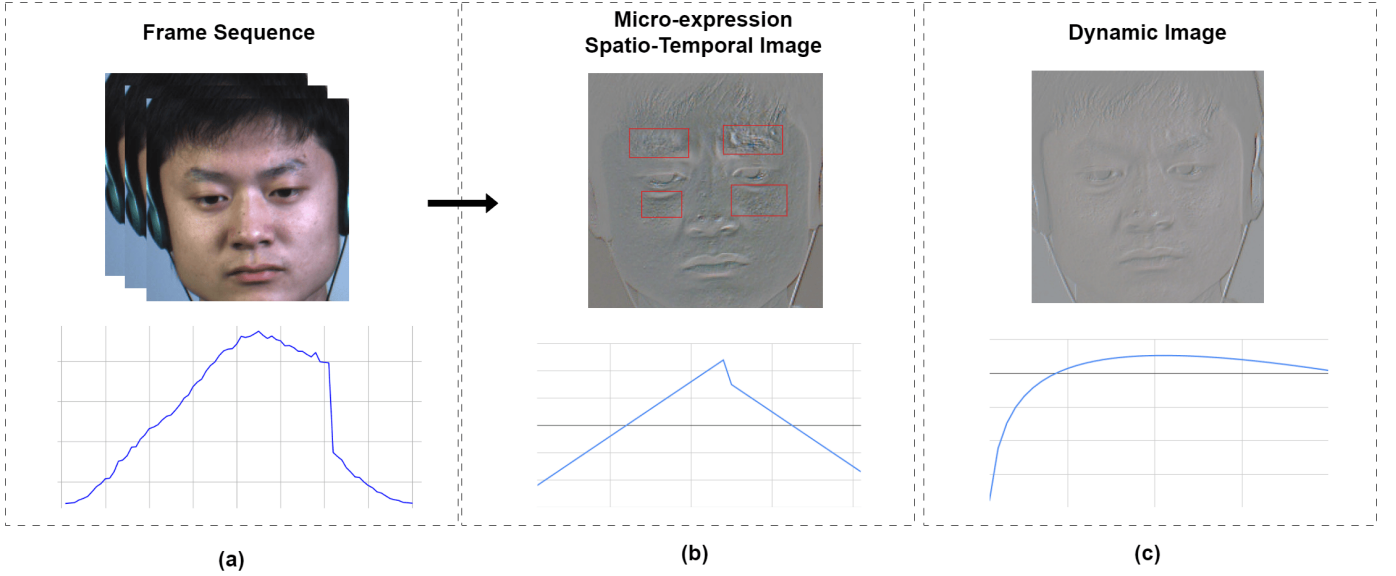


Fig. 2: MESTI and Dynamic Image and their frame coefficients in Ranking Function.

the intensity gradually increases from the first frame (onset), peaks at the apex frame, and then gradually decreases toward the final frame (offset) of the micro-expression. Therefore, in this study, we aim to model the motion characteristics of micro-expressions within the temporal encoding process to construct a micro-expression image from the video.

Temporal encoding is implemented by generating a ranking score that simulates the motion intensity of the micro-expression in a straightforward manner during the rank pooling process. Let  $I_a$  defined as the apex frame, where the motion intensity of the micro-expression reaches its maximum. Given any two frames  $I_q, I_t$ , the frame closer to the apex frame is assigned a higher ranking score in our ranking function.

Thus, for any pair of frames  $\{I_q, I_t\}$  such that  $|a - q| \leq |a - t|$ , establishing the ranking score:  $S(q|d) > S(t|d)$ . Accordingly, Equation 2 is further expanded as Equation 3:

$$E(d) = \frac{\lambda}{2} \|d\|^2 + \frac{2}{T(T-1)} \times \sum_{|a-q| \leq |a-t|} \max\{0, 1 - S(q|d) + S(t|d)\}. \quad (3)$$

The first term in Equation 3 is the standard quadratic regularizer used in SVMs. The second term is a hinge-loss function that soft-counts how many pairs of frames are incorrectly ranked by the scoring function. To solve the equations involving Equation 1 and Equation 2, the ARP method [28] is used. Starting with  $d = \vec{0}$ , the first approximated solution obtained by gradient descent is:

$$d^* = \vec{0} - \eta \nabla E(d)|_{d=\vec{0}} \propto -\nabla E(d)|_{d=\vec{0}} \text{ for any } \eta > 0$$

where:

$$\nabla E(\vec{0}) \propto \sum_{|a-q| > |a-t|} \nabla \max\{0, 1 - S(q|d) + S(t|d)\}|_{d=\vec{0}}$$

$$= \sum_{|a-q| > |a-t|} \nabla \langle d, \psi(I_t) - \psi(I_q) \rangle = \sum_{|a-q| > |a-t|} (\psi(I_t) - \psi(I_q))$$

$d^*$  can be expanded as follows:

$$\begin{aligned} d^* &\propto \sum_{|a-q| > |a-t|} (\psi(I_q) - \psi(I_t)) \\ &= \begin{cases} \sum_{q>t} (\psi(I_q) - \psi(I_t)) & \text{if } 1 \leq t \leq a \\ \sum_{q>t} (\psi(I_t) - \psi(I_q)) & \text{if } a < t \leq T \end{cases} \\ &= \begin{cases} \sum_{t=1}^a \alpha_t \psi(I_t) & \text{if } 1 \leq t \leq a \\ \sum_{t=a+1}^T \alpha_t \psi(I_t) & \text{if } a < t \leq T \end{cases} \end{aligned}$$

where  $\alpha_t$  is scalar coefficients. By expanding the sum:

*When the action in the range of onset frame and apex frame ( $1 \leq t \leq a$ ):*

$$\begin{aligned} \sum_{q>t} \psi(I_q) - \psi(I_t) &= (\psi(I_2) - \psi(I_1)) \\ &\quad + (\psi(I_3) - \psi(I_1)) + (\psi(I_3) - \psi(I_2)) \\ &\quad + \dots + \end{aligned}$$

$$(\psi(I_a) - \psi(I_1)) + (\psi(I_a) - \psi(I_2)) + \dots + (\psi(I_a) - \psi(I_{a-1}))$$

*When the action in the range of apex frame and offset frame ( $a < t \leq T$ ):*

$$\begin{aligned} \sum_{q>t} \psi(I_t) - \psi(I_q) &= (\psi(I_{a+1}) - \psi(I_{a+2})) \\ &\quad + (\psi(I_{a+1}) - \psi(I_{a+3})) + (\psi(I_{a+2}) - \psi(I_{a+3})) \\ &\quad + \dots + \\ &\quad (\psi(I_{a+1}) - \psi(I_T)) + (\psi(I_{a+2}) - \psi(I_T)) + \dots + (\psi(I_{T-1}) - \psi(I_T)) \end{aligned}$$

Finally, the coefficient  $\alpha_t$  can be efficiently computed in two scenarios by aggregating the coefficients of  $\psi(I_t)$  along with their respective positive and negative signs:

$$\alpha_t = \begin{cases} (t-1) - (a-t) & \text{if } 1 \leq t \leq a \\ (T-t) - (t-a-1) & \text{if } a < t \leq T \end{cases}$$

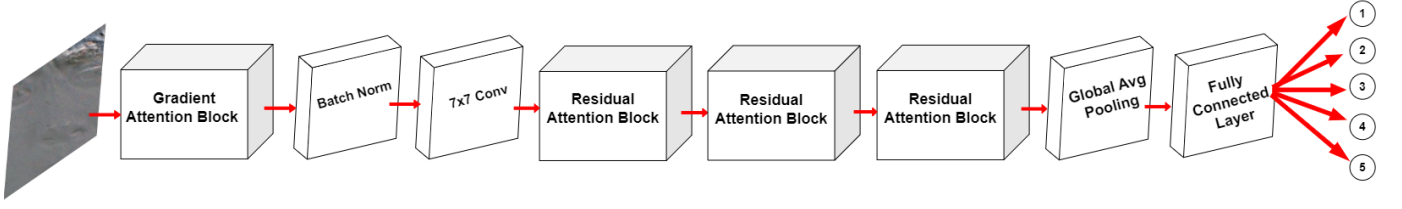


Fig. 3: The architecture of the proposed Micro-Expression Gradient Attention Network (MEGANet)

$$\Rightarrow \alpha_t = \begin{cases} 2t - a - 1 & \text{if } 1 \leq t \leq a \\ T - 2t + a + 1 & \text{if } a < t \leq T \end{cases} \quad (4)$$

Hence  $d^*$  can be present as the rank pooling operator after using ARP calculation:

$$d^* \approx \hat{\rho}(I_1, \dots, I_T; \psi) = \begin{cases} \sum_{t=1}^a \alpha_t \psi(I_t) & \text{if } 1 \leq t \leq a \\ \sum_{t=a+1}^T \alpha_t \psi(I_t) & \text{if } a < t \leq T \end{cases} \quad (5)$$

Finally, the MESTI construction is approximated by multiplying the feature vector representing the RGB component of each frame at time  $t$  with the  $\alpha$  coefficient provided in Equation 4.

The MESTI construction result is shown in Figure 2b using frame sequence (Figure 2a) as input. From the input frame sequence, we represent and observe the motion intensity of the ME representation and have the graph below. The MESTI construction results show that, firstly, our method generates a ranking function that better simulates the nature of the micro-expression motion. Second, through the visual representation results, MESTI has shown more clearly the action units in the micro-expression on the final image constructed compared to the traditional dynamic image method as showed in Figure 2c.

### B. Micro-expression Gradient Attention Networks

The challenge in micro-expression recognition lies in capturing the subtle, transient spatiotemporal patterns that characterize micro-expressions, which often involve subtle intensity changes that conventional CNNs struggle to detect. These expressions are fleeting, making it difficult for traditional methods to effectively focus on the most critical regions of motion. To address this, MEGANet is proposed, a MER network that aims to enhance the detection of micro-expressions by directing attention to areas with significant gradient changes. The core idea behind MEGANet is to combine gradient-guided attention with spatial self-attention, enabling the network to focus on both fine-grained motion transitions and the broader spatial context.

The proposed architecture consists of two key components as showed in Figure 3: the Gradient Attention Block and the Residual Attention Block. The Gradient Attention Block focuses on amplifying micro-intensity transitions by computing both horizontal and vertical gradients to identify regions with sharp intensity changes. This block generates an attention map through convolution and sigmoid activation, which is then multiplied with the input, enabling the network to prioritize areas with significant micro-movement. The

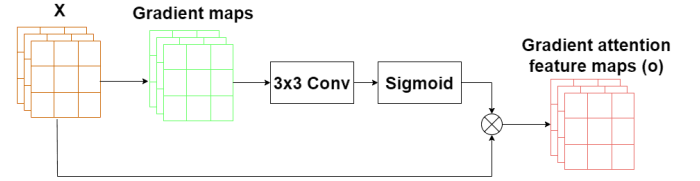


Fig. 4: Gradient Attention Block

Residual Attention Block, on the other hand, further refines the features by considering the spatial context, ensuring that important structural information is preserved during the feature extraction process. The overall network follows a structured pipeline comprising multiple processing layers:

- **Input layer:** The input to the network is an RGB image of size  $224 \times 224 \times 3$ .
- **Gradient Attention Block:** Computes spatial gradients to enhance subtle micro-expression features. A convolutional layer followed by a sigmoid activation generates an attention map, which is multiplied with the original input to highlight key regions.
- **Convolutional Feature Extraction:** A  $7 \times 7$  convolutional layer with 64 filters, followed by batch normalization, ReLU activation, and max pooling, extracts low-level spatial features from the input image.
- **Residual-Attention Blocks:** Three residual attention blocks process the feature maps hierarchically. Each block consists of two  $3 \times 3$  convolutional layers, batch normalization, ReLU activation, and a residual connection. A self-attention module is integrated to capture long-range spatial dependencies.
- **Global Feature Aggregation:** A global average pooling layer compresses the spatial feature maps into a compact feature vector, significantly reducing the number of parameters while retaining crucial information.
- **Fully Connected Layer and Classification:** The final feature vector is passed through a fully connected (FC) layer and a softmax activation function.

This architecture effectively captures micro-expression dynamics by leveraging gradient-based attention and residual learning, improving the network's ability to recognize subtle facial movements.

1) *Gradient Attention Block:* This block, illustrated in Figure 4, explicitly models horizontal and vertical intensity gradients to localize micro-expression regions. Given an input image  $X \in \mathbb{R}^{B \times C \times H \times W}$ , horizontal and vertical gradients at



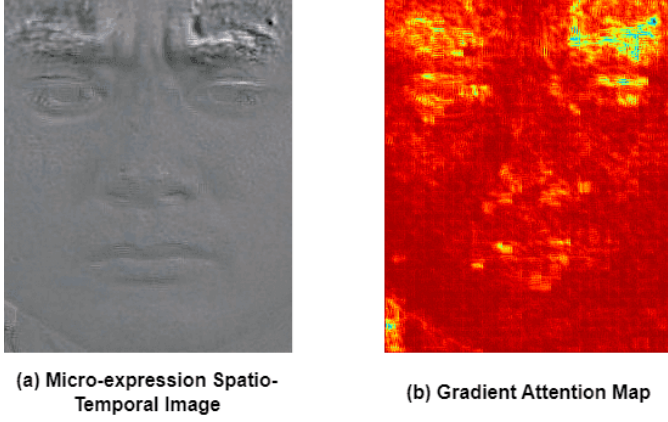


Fig. 5: The corresponding Gradient Attention map is generated with the input MESTI.

the spatial location  $(i, j)$  are computed as:

$$\begin{aligned} G_x(i, j) &= \|X(i, j+1) - X(i, j)\|_{\text{pad}} \\ G_y(i, j) &= \|X(i+1, j) - X(i, j)\|_{\text{pad}} \end{aligned} \quad (6)$$

where  $G_x, G_y \in \mathbb{R}^{B \times C \times H \times W}$  and  $\|\cdot\|_{\text{pad}}$  denotes zero-padded absolute differences. Combined gradient maps are generated through element-wise summation:

$$G_{\text{combined}} = G_x \oplus G_y \quad (7)$$

The gradient map is then processed through a learnable  $3 \times 3$  convolutional filter  $W_g$  ( $W_g \in \mathbb{R}^{1 \times C \times 3 \times 3}$ ), followed by sigmoid activation:

$$F_{\text{attn}} = \sigma(W_g * G_{\text{combined}}) \quad (8)$$

The final output is obtained via element-wise multiplication:

$$Y = X \odot F_{\text{attn}} \quad (9)$$

This attention map emphasizes regions with significant intensity transitions critical for micro-expression analysis. Figure 5 illustrate the gradient attention map constructed from our proposed MESTI as input image and gradient attention block.

2) *Residual - Attention Block*: Our Residual - Attention Block is illustrated in Figure 6, building upon residual connection and SAGAN's self-attention [44], this block aims to integrate self-attention into a residual framework to enhance spatial context modeling. Let  $F(X)$  denote the transformation by two convolutional layers:

$$\begin{aligned} F(X) &= \text{BN}_2(\text{Conv}_2(\text{RELU}(\text{BN}_1(\text{Conv}_1(X)))) \\ \text{Conv}_1 &: \mathbb{R}^{B \times C_{\text{in}} \times H \times W} \rightarrow \mathbb{R}^{B \times C_{\text{out}} \times H' \times W'} \\ \text{Conv}_2 &: \mathbb{R}^{B \times C_{\text{out}} \times H' \times W'} \rightarrow \mathbb{R}^{B \times C_{\text{out}} \times H' \times W'} \end{aligned} \quad (10)$$

A shortcut connection handles dimension mismatches:

$$X_{\text{shortcut}} = \begin{cases} \text{Conv}_{1 \times 1}(X) \\ X \end{cases} \quad (11)$$

The residual output becomes:

$$X_{\text{res}} = X_{\text{shortcut}} + F(X) \quad (12)$$

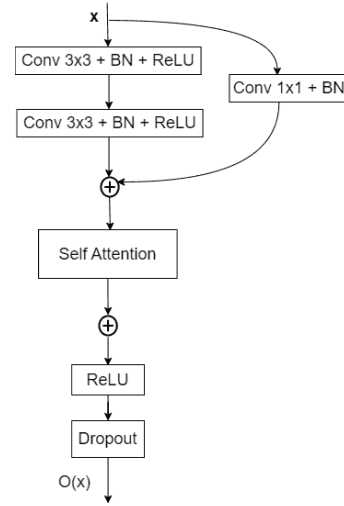


Fig. 6: Residual-Attention Block

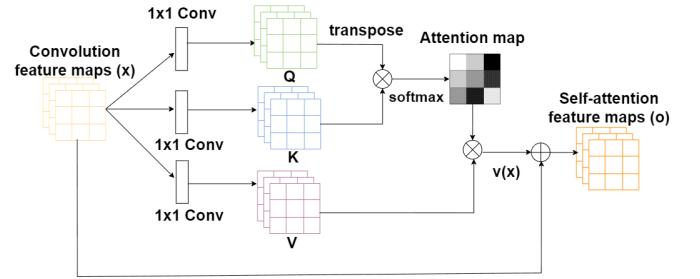


Fig. 7: Self-attention based on SAGAN

Followed by Self-Attention Module proposed by SAGAN illustrated in Figure 7, specifically:

$$\begin{aligned} Q &= \text{Conv}_{1 \times 1}(X_{\text{res}}), \quad Q \in \mathbb{R}^{B \times \frac{C}{8} \times HW} \\ K &= \text{Conv}_{1 \times 1}(X_{\text{res}}), \quad K \in \mathbb{R}^{B \times \frac{C}{8} \times HW} \\ \mathcal{E} &= \text{softmax}(Q^T K) \\ V &= \text{Conv}_{1 \times 1}(X_{\text{res}}), \quad V \in \mathbb{R}^{B \times C \times HW} \\ Y_{\text{attn}} &= \gamma(V\mathcal{E}^T), \quad \gamma \text{ is learnable} \end{aligned} \quad (13)$$

Finally:

$$Y = \text{Dropout}(\text{ReLU}(Y_{\text{attn}})) \quad (14)$$

### III. EXPERIMENTS AND RESULTS

#### A. Experiment scenarios and objectives

To evaluate the effectiveness of the proposed method for MER, which includes the MESTI as input representation, the MEGANet as MER network, and the combined approach of MESTI and MEGANet, three experimental scenarios were conducted to assess the performance of each proposed component:

**Experiment 01:** This experiment aims to evaluate the effectiveness of the MESTI input representation. Specifically, it compares MESTI with other input modalities previously used in MER studies, such as Apex Frame, Optical Flow, Dynamic Image, Active Image, and Affective Image. Furthermore, the experiment continues by replacing the input in previously

published MER networks with MESTI to investigate whether MESTI improves MER performance in these prior works.

**Experiment 02:** This experiment evaluates the performance of MEGANet in MER. MEGANet is used as a MER network using Dynamic Image input, and its performance is compared with other studies that utilized Dynamic Image. Additionally, the experiment extends to test MEGANet using MESTI as input, with three corresponding MER networks: VGG19, ResNet + Micro-attention, and MEGANet.

**Experiment 03:** This experiment assesses the overall effectiveness of the proposed MER method, combining MESTI and MEGANet. The results of this experiment are compared with previously published MER methods to demonstrate the superiority of the proposed approach.

### B. Dataset & Data preprocessing

1) *Datasets:* The experiments are conducted on two publicly available micro-expression recognition datasets, namely CASME II and SAMM, which are widely used as standard benchmarks for MER and for comparison with previous studies.

- **CASME II:** Part of the Chinese Academy of Sciences Micro-expression (CASME) dataset series, which includes CASME [42], CASME II [35], and CASME<sup>2</sup> [43]. Among these, CASME II is the most widely used dataset for micro-expression recognition tasks due to its significant improvements in both quantity and quality compared to the original CASME. CASME II contains a higher number of samples with more refined annotations, making it a reliable benchmark for evaluating micro-expression recognition networks. In contrast, CASME<sup>2</sup> is specifically designed for micro-expression spotting rather than recognition. It contains samples with longer durations and a lower frame rate, making it more suitable for identifying the precise temporal locations of micro-expressions within video sequences. This distinction highlights CASME II's relevance and dominance in the context of micro-expression recognition tasks. CASME II consists of 247 micro-expressions collected from 26 subjects. The dataset was recorded using a high-speed camera at 200 frames per second (fps), and the face regions were cropped to a resolution of  $280 \times 340$  pixels. These high frame rates and precise annotations make CASME II particularly well-suited for capturing the subtle and fleeting nature of micro-expressions.
- **SAMM:** Another widely used dataset in micro-expression recognition research. It comprises 159 micro-expression (ME) samples collected from 32 participants. The dataset was captured using a grayscale camera operating at 200 frames per second (fps) under controlled lighting conditions to prevent flickering. This high-speed recording ensures that subtle micro-expressions are accurately captured and preserved. A notable strength of SAMM lies in its ethnic diversity. Unlike earlier datasets, which often lacked representation, SAMM features participants from 13 different ethnic backgrounds. This diversity enhances the dataset's robustness and generalizability, making it a

valuable resource for developing and evaluating micro-expression recognition networks across varied populations.

2) *Data preprocessing:* To ensure a fair comparison, the data preprocessing steps are minimalized, limiting them to face cropping, histogram equalization and resizing the images to dimensions appropriate for each network's input requirements. This minimalistic approach eliminates potential biases from complex preprocessing techniques, allowing us to isolate and highlight the contributions of each input modality to overall network performance.

The original five emotion labels are retained as annotated in both datasets. Therefore, in the CASME II dataset, the micro-expression labels include disgust (60), happiness (33), other (102), repression (27), and surprise (25). The SAMM dataset consists of the following emotion labels: anger (57), happiness (26), contempt (12), surprise (15), and other (49).

### C. Experimental settings

1) *Experiment 01:* To ensure a fair comparison of the effectiveness of all input modalities, a common procedure is applied to all modalities. A train-test split protocol is used, with 90% for training and 10% for testing. The input is sequentially fed into three widely recognized deep learning networks: VGG19, ResNet50, and EfficientNetB0. This standardized approach minimizes external factors that could influence performance outcomes, allowing the observed differences to be directly attributed to the input modality itself.

MESTI is further used as an alternative input for the MER networks employed in two prior studies. To ensure fairness and the significance of the comparison results, we implement the experimental method in the same manner as described in their studies. Both studies used the Leave-One-Subject-Out (LOSO) protocol for evaluation.

2) *Experiment 02:* MEGANet is evaluated using two input modalities: Dynamic Image and MESTI, as both modalities aim to represent a video as a single image. For the Dynamic Image input, MEGANet is compared with typical architectures that use Dynamic Image and evaluated using the LOSO protocol to ensure fairness. Building on the previous experiment, MEGANet is then directly compared with VGG19 and ResNet + Micro-attention, also using the LOSO protocol for evaluation and the MESTI input.

3) *Experiment 03:* This experiment is designed to evaluate the proposed method in this paper, using MESTI as the input and MEGANet as the MER network. The experiment is conducted using the LOSO protocol for evaluation to ensure a meaningful comparison with previously published methods.

4) *Specific configuration and training methodology:* The following configuration and training methodology were used in this study:

- **Data Augmentation:** The dataset is augmented using horizontal flipping and rotations at  $5^\circ$  and  $10^\circ$  (both clockwise and counterclockwise).
- **Loss Function:** Focal Loss was used to address class imbalance and improve the network's focus on hard-to-classify samples.

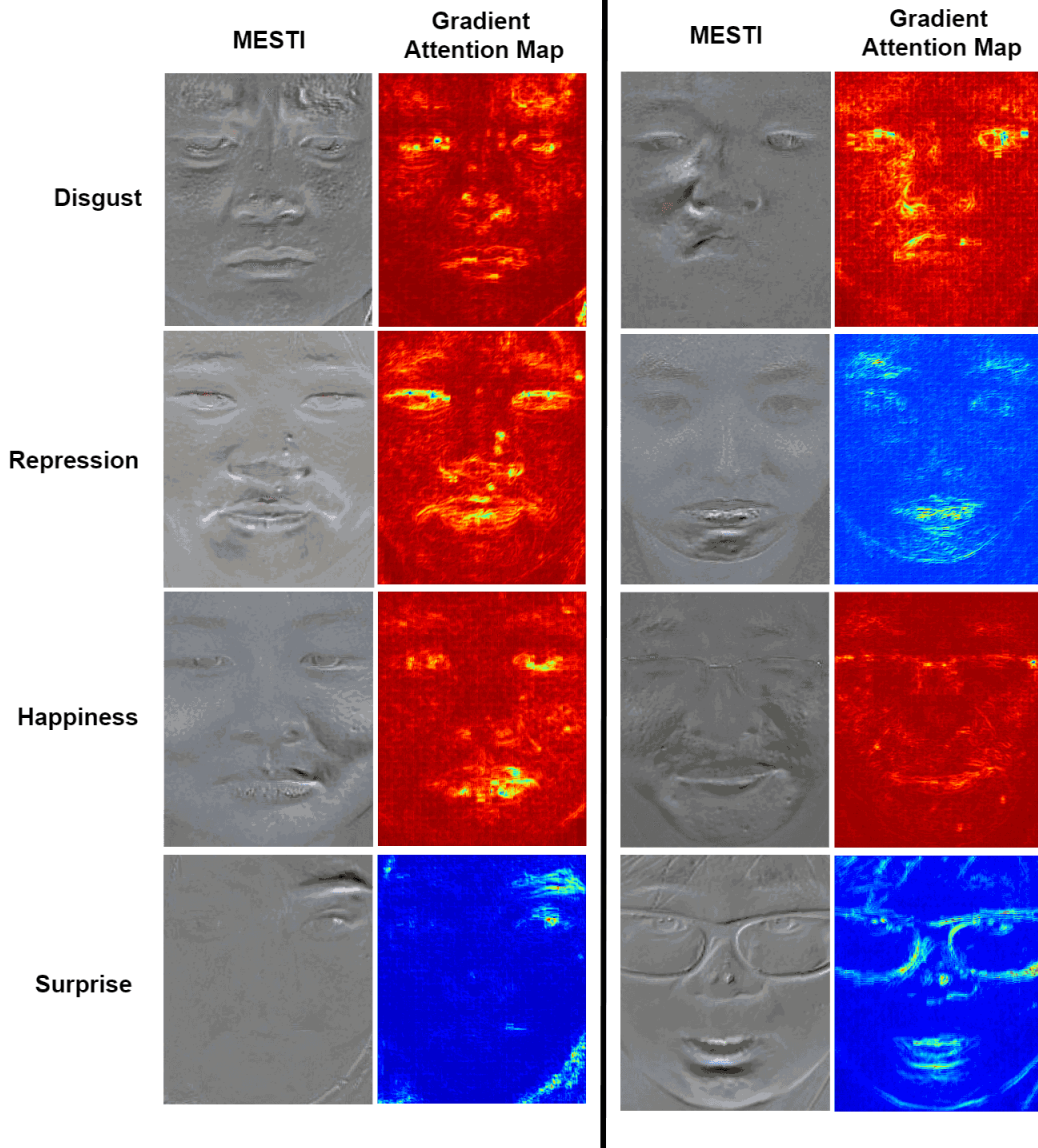


Fig. 8: Visualization of MESTI and corresponding Gradient Attention Map characterize each emotion of micro-expression (Best viewed in color)

TABLE I: Comparison of input modalities in Micro-Expression Recognition (MER) with Train-Test split protocol.

Input modality for MER		Network		
		VGG19 (CASMEII - SAMM)	Resnet50 (CASMEII - SAMM)	EfficientnetB0 (CASMEII - SAMM)
Static	Apex frame	50.00% - 43.75%	46.15% - 50.00%	34.62% - 43.75%
Dynamic	Optical flow (Onset - Apex)	50.00% - 50.00%	46.15% - 37.50%	26.92% - 43.75%
	Optical flow (Apex - Offset)	53.85% - 50.00%	34.62% - 43.75%	46.15% - 43.75%
	Dynamic image	57.69% - 50.00%	53.85% - 37.50%	53.85% - <b>50.00%</b>
	Affective motion image	50.00% - 43.75%	53.85% - 50.00%	46.15% - 43.75%
	Active image	48.00% - 57.14%	44.00% - 50.00%	52.00% - 48.00%
	<b>MESTI (ours)</b>	<b>73.08% - 62.5%</b>	<b>65.38% - 56.25%</b>	<b>61.54% - 50.00%</b>

- **Optimizer:** The Adam optimizer was employed with a learning rate of and weight decay of to optimize the network.
- **Training Duration:** The network was trained for 50 epochs to ensure convergence and adequate learning.

- **Metric:** The primary evaluation metric is accuracy. In the context of the LOSO protocol, accuracy is calculated as Equation 15:

$$Accuracy = \frac{\sum_{i=1}^S T_i}{\sum_{i=1}^S N_i} \times 100\% \quad (15)$$



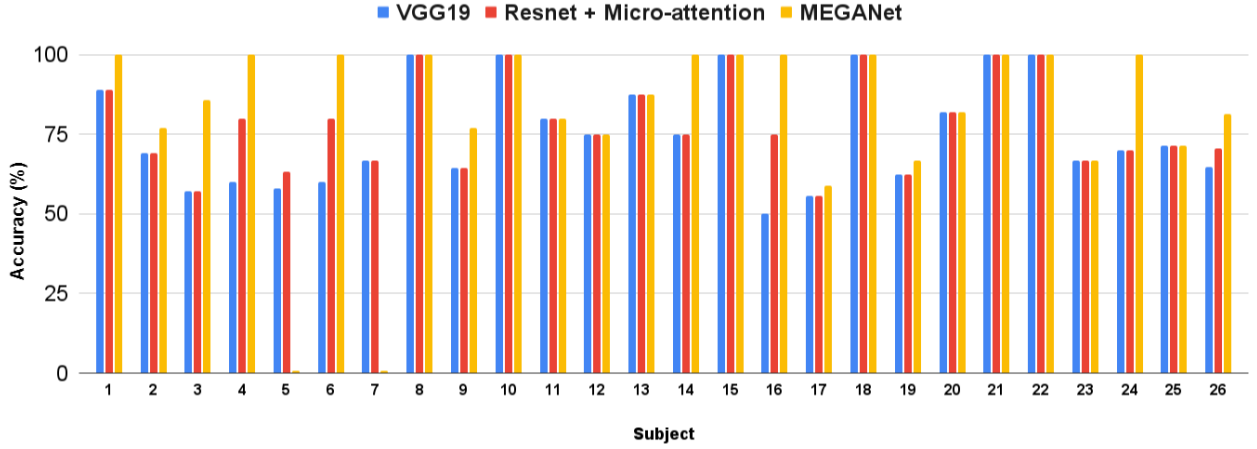


Fig. 9: Results of each subject on CASMEII dataset.

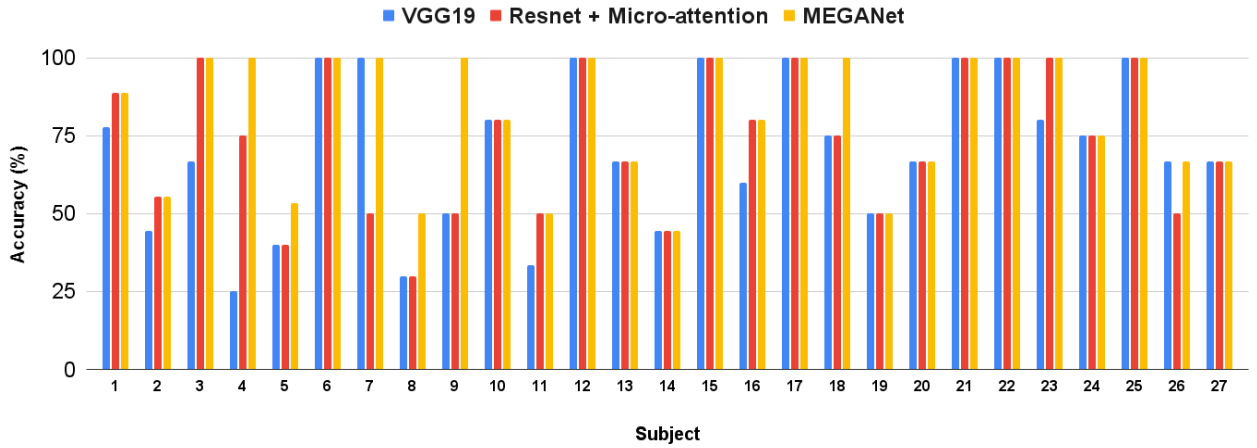


Fig. 10: Results of each subject on SAMM dataset.

where  $T_i$  and  $N_i$  are the number of correctly predicted samples and the number of samples, respectively, when the samples of the  $i$ -th subject is used as the test set.

#### D. Results

1) *Visual representation*: The visual results of MESTI and its corresponding Gradient Attention Map are shown in Figure 8 to observe how MESTI captures the characteristic features of each micro-expression emotion type and how the Gradient Attention Map highlights the regions of interest within MESTI. A key observation is that MESTI effectively captures and highlights the defining motion patterns of micro-expressions, making them perceptible to the human eye in a single image representation.

More specifically, both MESTI and the Gradient Attention Map successfully depict the characteristic Action Units corresponding to different micro-expression emotions. For Disgust, the key motion regions primarily appear around the eyebrows, one side of the nose, and the corners of the mouth. Repression manifests as subtle downward movements on both sides of the mouth and the chin. Happiness is expressed by an upward

motion at the corners of the mouth, whereas Surprise is predominantly reflected in eyebrow elevation and lower lip movement. These findings highlight the capability of MESTI to encode motion dynamics effectively in a compact and visually interpretable format.

2) *Experiment 01*: Table I summarizes the comparative performance of various input modalities in the micro-expression recognition (MER) task, evaluated using deep learning network on the CASMEII and SAMM datasets. The results consistently demonstrate that MESTI outperforms all other input modalities across the three widely used CNN architectures: VGG19, ResNet50, and EfficientNetB0. Specifically, MESTI achieves the highest accuracy of 73.08% on CASMEII and 62.5% on SAMM with VGG19, surpassing the second-best input modality (Dynamic Image) by 15.39% and 12.5%, respectively. This superior performance underscores MESTI's effectiveness in capturing subtle motion features, which are crucial for micro-expression recognition.

The second-best performing input modalities vary across networks but generally include Dynamic Image, Optical Flow, and Apex Frame, which have been commonly used in previous

TABLE II: Comparison of state-of-the-art methods and input modalities for MER with LOSO protocol in CASMEII Dataset.

No	Method	Network architecture	Input modality	Category	Accuracy
1	MER-GCN [53]	3DCNN	Action unit	5	42.03%
2	MER-GCN [53]	GCN	Action unit	5	42.71%
3	SelectiveCNN [45]	CNN	Difference image	5	47.3%
4	LEARNet [51]	VGG19	Dynamic Image	5	51.02%
5	Capsnet [50]	CapsNet	Apex image	5	51.62%
6	Capsnet [50]	CNN	Apex image	5	55.28%
7	AffectiveNet [55]	Affective net	Affective-motion image	4	61.02%
8	Active Imaging [57]	OrigNet	Active Image	5	62.09%
9	OFF-ApexNet [46]	OFF-Apex Net	Apex image	5	62.18%
10	LGCCCon [54]	VGG16 + GI path + LI path	Apex image	5	65.02%
11	Micro-attention [48]	Resnet + Micro-attention	Apex image	5	65.9%
12	FeatRef [41]	InceptionNet + FeatRef	Optical Flow	5	68.38%
13	GEME [56]	Dualstream-Multitask	Dynamic Image	5	75.2%
14	AMAN [52]	CNN + Attention Block	Image sequence	5	75.4%
15	LEARNet [51]	CNN-LEARNet	Dynamic Image	5	76.57%
16	<b>Ours</b>	<b>MEGANet</b>	<b>Dynamic Image</b>	<b>5</b>	<b>68.16%</b>
17	<b>Ours</b>	<b>VGG19</b>	<b>MESTI</b>	<b>5</b>	<b>69.39%</b>
18	<b>Ours</b>	<b>Resnet + Micro-attention [48]</b>	<b>MESTI</b>	<b>5</b>	<b>71.02%</b>
19	<b>Ours</b>	<b>MEGANet</b>	<b>MESTI</b>	<b>5</b>	<b>78.78%</b>

TABLE III: Comparison of state-of-the-art methods and input modalities for MER with LOSO protocol in SAMM Dataset.

No	Method	Network architecture	Input modality	Category	Accuracy
1	Active Imaging [57]	OrigNet	Active Image	5	34.02%
2	LGCCCon [54]	VGG16 + GI path + LI path	Apex image	5	40.9%
3	LEARNet [51]	VGG19	Dynamic Image	5	43.23%
4	LEARNet [51]	CNN-LEARNet	Dynamic Image	5	44.85%
5	Micro-attention [48]	Resnet + Micro-attention	Apex image	5	48.5%
6	GEME [56]	Dualstream-Multitask	Dynamic Image	5	55.88%
7	AffectiveNet [55]	Affective net	Affective-motion image	4	58.12%
8	FeatRef [41]	InceptionNet + FeatRef	Optical Flow	5	60.13%
9	AMAN [52]	CNN + Attention Block	Image sequence	5	68.85%
10	<b>Ours</b>	<b>MEGANet</b>	<b>Dynamic Image</b>	<b>5</b>	<b>63.97%</b>
11	<b>Ours</b>	<b>VGG19</b>	<b>MESTI</b>	<b>5</b>	<b>60.29%</b>
12	<b>Ours</b>	<b>Resnet + Micro-attention [48]</b>	<b>MESTI</b>	<b>5</b>	<b>63.24%</b>
13	<b>Ours</b>	<b>MEGANet</b>	<b>MESTI</b>	<b>5</b>	<b>71.32%</b>

MER research. For example, Dynamic Image achieves 57.69% (CASMEII) and 50.00% (SAMM) with VGG19, while Optical Flow (Apex-Offset) achieves 53.85% (CASMEII) and 50.00% (SAMM). However, these modalities fall short of MESTI's performance due to their inability to fully capture the transient and subtle nature of micro-expressions. Static images like the Apex Frame, while computationally efficient, lack temporal information, leading to suboptimal accuracy (50.00% on CASMEII and 43.75% on SAMM with VGG19). Optical Flow, though effective in encoding motion, is susceptible to noise from lighting variations and head movements, particularly for low-amplitude micro-expressions.

For the SAMM dataset, the overall recognition performance is lower compared to CASMEII across all input modalities, a trend consistent with previous studies due to SAMM's greater diversity and complexity. Despite this challenge, MESTI continues to demonstrate superior recognition capabilities,

achieving 62.5% with VGG19 and 56.25% with ResNet50, reinforcing its robustness across different datasets and deep learning architectures.

To further validate MESTI's effectiveness, we investigated whether its superior performance was specific to our proposed pipeline or if it could enhance other established MER architectures. The original input modalities are replaced by two previously published works with MESTI: VGG19 (originally using Dynamic Image) and ResNet + Micro-Attention (originally using Apex Frame). For VGG19, replacing the input with MESTI improved recognition accuracy from 51.02% to 69.39% on CASMEII and from 43.23% to 60.29% on SAMM. Similarly, for ResNet + Micro-Attention, using MESTI as input improved accuracy from 65.90% to 71.02% on CASMEII and from 48.5% to 63.24% on SAMM. These results confirm that MESTI not only enhances our proposed network but also significantly improves the performance of other MER archi-

tures, demonstrating its capability to effectively represent micro-expression dynamics in a single image.

3) *Experiment 02*: Proposed MEGANet is evaluated by comparing it to other architectures when using MESTI as input. Figures 9 and 10 illustrate the LOSO validation results for individual subjects, confirming that MEGANet outperforms both VGG19 and ResNet + Micro-Attention when trained on MESTI. This indicates that the integration of MESTI with MEGANet's Gradient Attention mechanism leads to a substantial performance gain. The results, shown in Row 19 of Table II and Row 13 of Table III, demonstrate that the combination of MEGANet + MESTI achieves state-of-the-art performance, reaching 78.78% accuracy on CASMEII and 71.32% on SAMM, surpassing previously published methods.

To further assess MEGANet's adaptability, an additional experiment is conducted using Dynamic Image as input, comparing its performance with other Dynamic Image-based architectures. On the SAMM dataset, MEGANet achieved 63.97% accuracy, surpassing all other methods utilizing Dynamic Image as input. On CASMEII, MEGANet attained 68.16% accuracy, which, while slightly lower than LEARNet (76.57%) and GEME (75.2%), still demonstrated highly competitive performance. These results suggest that while MEGANet is optimized for MESTI, it remains highly effective even when using Dynamic Image. This underscores the robustness of MEGANet's Gradient Attention mechanism, which enhances the extraction of micro-movements across different input representations.

4) *Experiment 03*: The synergy between MESTI and MEGANet establishes a new benchmark in MER. As shown in Table II, the proposed method outperforms all prior works, including AMAN [52] (75.4%) and GEME [56] (75.2%), by 3.38% on CASMEII. On SAMM (Table III), it achieves 71.32%, surpassing the second-best method (AMAN [52]: 68.85%) by 2.47%. This success is attributed to two key factors:

- MESTI's motion-specific encoding, which preserves spatiotemporal dynamics (Figure 2), and
- MEGANet's Gradient Attention mechanism, which focuses on intensity transitions (Figure 5) while residual blocks model long-range dependencies (Figure 6).

#### IV. CONCLUSION

In this work, we address the limitations of existing MER methodologies by introducing Micro-expression Spatio-Temporal Image as a novel input modality and Micro-expression Gradient Attention Network as a novel architecture. MESTI effectively encodes micro-movements into a single image, preserving both spatial and temporal features, while MEGANet utilizes a Gradient Attention mechanism to enhance the detection of subtle motion cues.

Our experimental results validate the effectiveness of MESTI by showing that it outperforms all other input modalities, including Apex Frame, Optical Flow, and Dynamic Image, across multiple deep learning networks. Furthermore, replacing the input of previously published MER architectures with MESTI results in significant improvements in recognition

accuracy, highlighting its broad applicability. Additionally, MEGANet achieves state-of-the-art performance, particularly when combined with MESTI, confirming its effectiveness in micro-expression analysis. Even when tested with Dynamic Image, MEGANet remains highly competitive, further reinforcing the robustness of its Gradient Attention mechanism. These findings establish MESTI and MEGANet as highly effective solutions for MER, significantly improving recognition accuracy. Future work could explore refining MESTI for real-time applications, integrating additional attention mechanisms, or leveraging larger-scale datasets to further advance micro-expression recognition systems.

#### REFERENCES

- [1] Nummenmaa, L., Saarimäki, H., Glereana, E., Gotsopoulos, A., Jääskeläinen, I., Harib, R., Samsa, M., Glerean, E., Hari, R., Hietanen, J. & Others Ekman, Paul (2007). *Emotions Revealed. Recognizing faces and feelings to improve communication and emotional life*. New York: Holt Paper-back, Montgomery, Arlene (2013) *Neurobiology Essentials for Clinicians. What every therapist needs to know*, New York, London, WW Nor.
- [2] Yan, W., Wu, Q., Liang, J., Chen, Y. & Fu, X. How Fast are the Leaked Facial Expressions: The Duration of Micro-Expressions. *Journal Of Non-verbal Behavior*. **37**, 217-230 (2013,12), <https://doi.org/10.1007/s10919-013-0159-8>
- [3] Matsumoto, D. & Hwang, H. Evidence for training the ability to read microexpressions of emotion. *Motivation And Emotion*. **35**, 181-191 (2011,6), <https://doi.org/10.1007/s11031-011-9212-2>
- [4] Ekman, P. Darwin, deception, and facial expression. *Ann N Y Acad Sci*. **1000** pp. 205-221 (2003,12)
- [5] Goh, K., Ng, C., Lim, L. & Sheikh, U. Micro-expression recognition: an updated review of current trends, challenges and solutions. *The Visual Computer*. **36**, 445-468 (2020,3), <https://doi.org/10.1007/s00371-018-1607-6>
- [6] Li, X., Hong, X., Moilanen, A., Huang, X., Pfister, T., Zhao, G. & Pietikäinen, M. Towards Reading Hidden Emotions: A Comparative Study of Spontaneous Micro-Expression Spotting and Recognition Methods. *IEEE Transactions On Affective Computing*. **9**, 563-577 (2018)
- [7] Yildirim, S., Chimeumanu, M. & Rana, Z. The influence of micro-expressions on deception detection. *Multimedia Tools And Applications*. **82**, 29115-29133 (2023,8), <https://doi.org/10.1007/s11042-023-14551-6>
- [8] Frank, M. & Svetieva, E. Microexpressions and Deception. *Understanding Facial Expressions In Communication: Cross-cultural And Multidisciplinary Perspectives*. pp. 227-242 (2015), <https://doi.org/10.1007/978-81-322-1934-7-11>
- [9] Endres, J. & Laidlaw, A. Micro-expression recognition training in medical students: a pilot study. *BMC Medical Education*. **9**, 47 (2009,7), <https://doi.org/10.1186/1472-6920-9-47>
- [10] Frank, M., Herbasz, M., Sinuk, K., Keller, A. & Nolan, C. I see how you feel: Training laypeople and professionals to recognize fleeting emotions. *The Annual Meeting Of The International Communication Association. Sheraton New York, New York City*. pp. 1-35 (2009)
- [11] Li, Y., Wei, J., Liu, Y., Kauttonen, J. & Zhao, G. Deep Learning for Micro-Expression Recognition: A Survey. *IEEE Transactions On Affective Computing*. **13**, 2028-2046 (2022)
- [12] Quang, N., Chun, J. & Tokuyama, T. CapsuleNet for Micro-Expression Recognition. *2019 14th IEEE International Conference On Automatic Face & Gesture Recognition (FG 2019)*. pp. 1-7 (2019), <https://doi.org/10.1109/FG.2019.8756544>
- [13] Li, Y., Huang, X. & Zhao, G. Can Micro-Expression be Recognized Based on Single Apex Frame?. *2018 25th IEEE International Conference On Image Processing (ICIP)*. pp. 3094-3098 (2018)
- [14] Nie, X., Takalkar, M., Duan, M., Zhang, H. & Xu, M. GEME: Dual-stream multi-task Gender-based micro-expression recognition. *Neurocomputing*. **427** pp. 13-28 (2021), <https://www.sciencedirect.com/science/article/pii/S0925231220316957>
- [15] Quynh Le, T., Tran, T. & Rege, M. Dynamic image for micro-expression recognition on region-based framework. *2020 IEEE 21st International Conference On Information Reuse And Integration For Data Science (IRI)*. pp. 75-81 (2020)
- [16] Verma, M., Vipparthi, S. & Singh, G. Non-Linearities Improve OrigNet based on Active Imaging for Micro Expression Recognition. (2020,7)

- [17] Wu, J., Xu, J., Lin, D. & Tu, M. Optical Flow Filtering-Based Micro-Expression Recognition Method. *Electronics*. **9** (2020), <https://www.mdpi.com/2079-9292/9/12/2056>
- [18] Hadid, A. The Local Binary Pattern Approach and its Applications to Face Analysis. *2008 First Workshops On Image Processing Theory, Tools And Applications*. pp. 1-9 (2008)
- [19] Ruiz-Hernandez, J. & Pietikäinen, M. Encoding Local Binary Patterns using the re-parametrization of the second order Gaussian jet. *2013 10th IEEE International Conference And Workshops On Automatic Face And Gesture Recognition (FG)*. pp. 1-6 (2013), <https://api.semanticscholar.org/CorpusID:6766879>
- [20] Wang, Y., See, J., Phan, R. & Oh, Y. LBP with Six Intersection Points: Reducing Redundant Information in LBP-TOP for Micro-expression Recognition. *Computer Vision – ACCV 2014*. pp. 525-537 (2015)
- [21] Huang, X., Wang, S., Zhao, G. & Pietikäinen, M. Facial Micro-Expression Recognition Using Spatiotemporal Local Binary Pattern with Integral Projection. (2015,12)
- [22] Huang, X., Zhao, G., Hong, X., Zheng, W. & Pietikäinen, M. Spontaneous facial micro-expression analysis using Spatiotemporal Completed Local Quantized Patterns. *Neurocomputing*. **175** pp. 564-578 (2016), <https://www.sciencedirect.com/science/article/pii/S0925231215015726>
- [23] Zeng, X., Zhao, X., Zhong, X. & Liu, G. A Survey of Micro-expression Recognition Methods Based on LBP, Optical Flow and Deep Learning. *Neural Processing Letters*. **55**, 5995-6026 (2023,10), <https://doi.org/10.1007/s11063-022-11123-x>
- [24] Barron, J., Fleet, D. & Beauchemin, S. Performance Of Optical Flow Techniques. *International Journal Of Computer Vision*. **12** pp. 43-77 (1994,2)
- [25] Liu, Y., Zhang, J., Yan, W., Wang, S., Zhao, G. & Fu, X. A Main Directional Mean Optical Flow Feature for Spontaneous Micro-Expression Recognition. *IEEE Transactions On Affective Computing*. **7**, 299-310 (2016)
- [26] Liong, S., See, J., Wong, K. & Phan, R. Less is more: Micro-expression recognition from video using apex frame. *Signal Processing: Image Communication*. **62** pp. 82-92 (2018), <https://www.sciencedirect.com/science/article/pii/S0923596517302436>
- [27] Happy, S. & Routray, A. Fuzzy histogram of optical flow orientations for micro-expression recognition. *IEEE Transactions On Affective Computing*. **10**, 394-406 (2017)
- [28] Bilen, H., Fernando, B., Gavves, E., Vedaldi, A. & Gould, S. Dynamic image networks for action recognition. *Proceedings Of The IEEE Conference On Computer Vision And Pattern Recognition*. pp. 3034-3042 (2016)
- [29] Fernando, B., Gavves, E., Oramas, J., Ghodrati, A. & Tuytelaars, T. Modeling Video Evolution for Action Recognition. *Proceedings Of The IEEE Conference On Computer Vision And Pattern Recognition (CVPR)*. (2015,6)
- [30] Fernando, B., Gavves, E., Oramas M., J., Ghodrati, A. & Tuytelaars, T. Rank Pooling for Action Recognition. *IEEE Transactions On Pattern Analysis And Machine Intelligence*. **39**, 773-787 (2017)
- [31] Smola, A. & Schölkopf, B. A tutorial on support vector regression. *Statistics And Computing*. **14** pp. 199-222 (2004)
- [32] Verma, M., Vipparthi, S. & Singh, G. AffectiveNet: Affective-Motion Feature Learning for Microexpression Recognition. *IEEE MultiMedia*. **28**, 17-27 (2021)
- [33] *2011 IEEE International Conference On Computer Vision Workshops (ICCV Workshops)*. pp. 868-875 (2011)
- [34] Bilen, H., Fernando, B., Gavves, E. & Vedaldi, A. Action Recognition with Dynamic Image Networks. *IEEE Trans. Pattern Anal. Mach. Intell.*. **40**, 2799-2813 (2018,12), <https://doi.org/10.1109/TPAMI.2017.2769085>
- [35] Yan, W., Li, X., Wang, S., Zhao, G., Liu, Y., Chen, Y. & Fu, X. CASME II: an improved spontaneous micro-expression database and the baseline evaluation. *PLoS One*. **9**, e86041 (2014,1)
- [36] Simonyan, K. & Zisserman, A. Very Deep Convolutional Networks for Large-Scale Image Recognition. (2015), <https://arxiv.org/abs/1409.1556>
- [37] He, K., Zhang, X., Ren, S. & Sun, J. Deep Residual Learning for Image Recognition. (2015), <https://arxiv.org/abs/1512.03385>
- [38] Tan, M. & Le, Q. EfficientNet: Rethinking Model Scaling for Convolutional Neural Networks. (2020), <https://arxiv.org/abs/1905.11946>
- [39] Wang, C., Peng, M., Bi, T. & Chen, T. Micro-attention for micro-expression recognition. *Neurocomputing*. **410** pp. 354-362 (2020), <https://www.sciencedirect.com/science/article/pii/S0925231220309711>
- [40] Davison, A., Lansley, C., Costen, N., Tan, K. & Yap, M. SAMM: A Spontaneous Micro-Facial Movement Dataset. *IEEE Transactions On Affective Computing*. **9**, 116-129 (2018)
- [41] Zhou, L., Mao, Q., Huang, X., Zhang, F. & Zhang, Z. Feature refinement: An expression-specific feature learning and fusion method for micro-expression recognition. *Pattern Recognition*. **122** pp. 108275 (2022), <https://www.sciencedirect.com/science/article/pii/S0031320321004556>
- [42] Yan, W., Wu, Q., Liu, Y., Wang, S. & Fu, X. CASME Database: a dataset of spontaneous micro-expressions collected from neutralized faces. *2013 10th IEEE International Conference And Workshops On Automatic Face And Gesture Recognition, FG 2013*. (2013,4)
- [43] Qu, F., Wang, S., Yan, W., Li, H., Wu, S. & Fu, X. CAS(ME)2: A Database for Spontaneous Macro-Expression and Micro-Expression Spotting and Recognition. *IEEE Transactions On Affective Computing*. **9** pp. 424-436 (2017,1)
- [44] Zhang, H., Goodfellow, I., Metaxas, D. & Odena, A. Self-Attention Generative Adversarial Networks. (2019), <https://arxiv.org/abs/1805.08318>
- [45] Patel, D., Hong, X. & Zhao, G. Selective deep features for micro-expression recognition. *2016 23rd International Conference On Pattern Recognition (ICPR)*. pp. 2258-2263 (2016)
- [46] Gan, Y., Liong, S., Yau, W., Huang, Y. & Tan, L. OFF-ApexNet on micro-expression recognition system. *Signal Processing: Image Communication*. **74** pp. 129-139 (2019)
- [47] Li, Q., Zhan, S., Xu, L. & Wu, C. Facial micro-expression recognition based on the fusion of deep learning and enhanced optical flow. *Multimedia Tools And Applications*. **78** pp. 29307-29322 (2019)
- [48] Wang, C., Peng, M., Bi, T. & Chen, T. Micro-attention for micro-expression recognition. *Neurocomputing*. **410** pp. 354-362 (2020)
- [49] Smola, A. & Schölkopf, B. A tutorial on support vector regression. *Statistics And Computing*. **14** pp. 199-222 (2004)
- [50] Liu, N., Liu, X., Zhang, Z., Xu, X. & Chen, T. Offset or onset frame: A multi-stream convolutional neural network with capsuleNet module for micro-expression recognition. *2020 5th International Conference On Intelligent Informatics And Biomedical Sciences (ICIIBMS)*. pp. 236-240 (2020)
- [51] Verma, M., Vipparthi, S., Singh, G. & Murala, S. LEARNNet: Dynamic Imaging Network for Micro Expression Recognition. *IEEE Transactions On Image Processing*. **29** pp. 1618-1627 (2020)
- [52] Wei, M., Zheng, W., Zong, Y., Jiang, X., Lu, C. & Liu, J. A Novel Micro-Expression Recognition Approach Using Attention-Based Magnification-Adaptive Networks. *ICASSP 2022 - 2022 IEEE International Conference On Acoustics, Speech And Signal Processing (ICASSP)*. pp. 2420-2424 (2022)
- [53] Lo, L., Xie, H., Shuai, H. & Cheng, W. MER-GCN: Micro-expression recognition based on relation modeling with graph convolutional networks. *2020 IEEE Conference On Multimedia Information Processing And Retrieval (MIPR)*. pp. 79-84 (2020)
- [54] Li, Y., Huang, X. & Zhao, G. Joint local and global information learning with single apex frame detection for micro-expression recognition. *IEEE Transactions On Image Processing*. **30** pp. 249-263 (2020)
- [55] Verma, M., Vipparthi, S. & Singh, G. AffectiveNet: Affective-motion feature learning for microexpression recognition. *IEEE MultiMedia*. **28**, 17-27 (2020)
- [56] Nie, X., Takalkar, M., Duan, M., Zhang, H. & Xu, M. GEME: Dual-stream multi-task Gender-based micro-expression recognition. *Neurocomputing*. **427** pp. 13-28 (2021), <https://www.sciencedirect.com/science/article/pii/S0925231220316957>
- [57] Verma, M., Vipparthi, S. & Singh, G. Non-Linearities Improve OrigNet based on Active Imaging for Micro Expression Recognition. *2020 International Joint Conference On Neural Networks (IJCNN)*. pp. 1-8 (2020)